Aggregation-induced Emission Fluorophore Doped Phosphate Glass: Toward Light-emitting Electrochemical Cells

Muzhi Cai, Laurent Calvez, Jean Rocherulle, Pierre-Antoine Bouit, Muriel Hissler, Hongli Ma, Claire Roiland, Vincent Dorcet, Junjie Zhang, Shiqing Xu, et al.

Aggregation-induced Emission Fluorophore Doped Phosphate Glass: Toward Light-emitting Electrochemical Cells

Muzhi Cai,[†,‡] Laurent Calvez,[‡] Jean Rocherulle,[‡] Pierre-Antoine Bouit,[‡] Muriel Hissler,[‡] Hongli Ma,[‡] Claire Roiland,[‡] Vincent Dorcet,[‡] Junjie Zhang,[†] Shiqing Xu,[†] and Xianghua Zhang[‡]*

†Institute of Optoelectronic Materials and Devices, Jiliang University, 310018, Hangzhou, China, People's Republic of China

‡ISCR (Institut des Sciences Chimiques de Rennes) UMR 6226, Univ Rennes, CNRS, F35000, Rennes, France

Corresponding author: laurent.calvez@univ-rennes1.fr

Keywords：optical materials; rapid-solidification, quenching; ionic conduction; optical properties

Abstract

Light-emitting electrochemical cell (LEC) is an easy-to-fabricate electroluminescent device, which in its simplest manifestation comprises an electroluminescence organic fluorophore and electrolytes as the active layer sandwiched between two electrodes. To date, the LEC exhibits poor operational stability, and the poor thermal stability of the electrolyte is a major cause of the

instability. Because most of the electrolytes utilized in LEC are organic electrolytes (polymer and ionic liquids), the thermal stability is difficult to improve on a large scale. Therefore, in this work, we devote to preliminarily explore the possibility of using an inorganic glass electrolyte for LEC application. Following this objective, hybrid glass based on organic fluorophore (π-extended phosphole sulfide **1**) doped inorganic phosphate amorphous matrix were successfully synthesized via the spark plasma sintering technology. The optical properties, microstructure and electrochemical properties of the hybrid glass were investigated respectively. The ionic conductivity of the glass host can reach 10^{-7} S/cm at room temperature, and the glass matrix contain aggregates of 1 of around 100 nm. Strong photoluminescence at 600 nm, characteristic of the organic fluorophore, was observed in the hybrid glass. The cyclic voltammetry performed on the hybrid glass shows a redox couple contribution of the organic fluorophore. This suggests **1** can complete the exchange of electric charges in the inorganic glass electrolyte, which is one of the fingerprints of the transient phenomena of a LEC.

INTRODUCTION

Light-emitting electrochemical cell (LEC), a single-layered lighting device consisting of an intimate blend of an emitter and an ionic electrolyte, offers many important advantages for solid-state lighting and display applications, such as high brightness, a large quantum efficiency, and a low turn-on voltage for light emission [1-4]. Since the discovery of the LEC concept in 1995, the impact of the ions on the device mechanism has carefully been studied [1], and it is rational to state that the last 20 years have been a successful test-bed time for the LEC technology [5-8]. However, LECs devices have exhibited a distinctly poor operational stability in comparison to the other

electroluminescence devices such as organic light-emitting diodes (OLED).[3, 9] Concerning this issue, Gao's group has reported that the role of both the substrate and the ionic poly-electrolyte are essential to control the device self-stability under different storage conditions[10], while Edman's group has demonstrated that the devices encapsulated has better stability than that of those nonencapsulated[11]. These researches imply that the operational stability of LEC is highly dependent on the chosen ionic electrolyte [4, 12, 13].

Recently, Edman's group investigated the self-heating phenomenon in LEC, and it was found that the luminance and current efficacy of LEC is improved with the increasing temperature, and the operational lifetime of LEC is dropping as well [14]. In addition, Costa's group found that the self-stability of iTMC-LEC depends on the kinds of electrolyte, and LEC based on ionic polyelectrolyte obtained by mixing trimethylolpropane ethoxylate (TMPE) with Lithium Triflate (LiOTf) or Potassium Triflate (KOTf) is more stable than that based on the ionic liquid (IL) 1-butyl-3-methylimidazolium hexafluorophosphate [15]. To some extent, the better stability of the electrolyte is, the longer the operational lifetime of LEC will be. To our best knowledge, most of the studies of electrolytes for LEC primarily focused on polymer electrolytes and IL exhibiting poor thermal stability [12,13]. Therefore, if an electrolyte with better thermal stability and relatively high ionic conductivity would considerably improve the operational lifetime of LEC devices.

Generally, inorganic glass electrolytes have better thermal stability and comparable ionic conductivity than those polymer electrolytes or IL mentioned above. However, one major challenge lies in the synthesis of organic emitter mixed within inorganic glass electrolyte because inorganic glass normally has a much higher synthesis temperature than the degradation temperature (T_d) of the most organic compounds. Fortunately, Spark Plasma Sintering (SPS) technology may overcome this problem through selecting suitable organic emitter and glass

components. In fact, as demonstrated in our previous work [16], glasses can be firstly synthesized at high temperature through conventional melt-quenching technique and then be crushed and shaped at temperature close to the glass transition temperature (T_g) by SPS. Therefore, inorganic glasses host must possess T_g as close to the T_d of an organic emitter as possible to prepare the mixed hybrid glass. Besides, the other physico-chemical characteristics of the inorganic electrolyte should match that of the organic emitter, such as the window of transparency, chemical compatibility, and electrochemical stability. Thus, an adequate selection of both organic molecules and phosphate glass composition must be realized to fulfill the requirements of LEC devices.

Some of us pioneered the use of π-conjugated phospholes for organic electronics and in particular for colored and white OLED [17]. We also showed that simple chemical modifications permit fine-tuning of the physical and chemical characteristics of phosphole-based π-conjugated systems including thermal stability, redox potentials, emission wavelength. In addition, such derivatives display higher luminescence in the aggregated-state compared to the diluted solution, a phenomenon usually called "aggregation-induced emission".[18] Ultimately, 1-Phenyl-2,5-bis(2-thienyl) thiooxo-phosphole **1**(Figure 1) fulfilling all the criteria discussed above was selected as prototypic fluorophore for this study.

On the other hand, phosphate glasses present a broad window of transparency from the UV to the near IR, and it also has moderate glass transition temperature around or below 300 °C [19]. This family of glass presents the great interest to be highly doped with small cations such as Li^+ in order to increase the ionic conductivity and in the meantime to decrease the network connectivity and the glass T_g. Therefore, in this work, we devote to preliminarily explore the possibility of synthesizing an inorganic phosphate glass electrolyte for LEC whose synthesis is compatible with the presence of an organic emitter such **1**, and the schematic process for the synthesizing of the

organic-inorganic hybrid glass is illustrated in Figure 1. The visible photoluminescence spectrum of the hybrid glass was performed. The microstructure of the hybrid glass was investigated by transmission electron microscope (TEM) and all-solid-state nuclear magnetic resonance (NMR). Further, the electrochemical properties of the hybrid glass were study through electrochemical impedance spectroscopy (EIS) and cyclic voltammetry (CV).

Material and methods

Synthesis

Selection of organic emitter

As mentioned above, the organic emitter used here is a 1-Phenyl-2,5-bis(2-thienyl)thiooxophosphole **1** with high luminescence efficiency in solid-state (l_{em} = 553 nm), reversible redox behavior and high degradation temperature (253°C, 10% weight loss).[20] It is worth noting that **1** was used to prepare the first OLED incorporating an organophosphorus emitter. The other characteristics of **1** are detailed in the Supporting Information Table S1.

Selection and synthesis of inorganic glass component

Binary alkali phosphate glasses with composition x%Li_2O-(100-x)%P_2O_5 (x=40, 50, 60) and ternary alkali phosphate glass with composition 25%Li_2SO_4-40%Li_2O-35%P_2O_5 (LPM) were prepared using the conventional melt-quench method. Batches consisting of Li_2O (or Li_2O and Li_2SO_4) and $NH_4H_2PO_4$ were calcined in alumina crucibles at 300 °C for 12 h under ambient atmosphere in a muffle furnace. Then, the calcined solid were melted in the air at 1100°C (900 °C for LPM) for 30 min. The glass melt was quenched on a steel plate at room temperature and then annealed at the glass transition temperature, 320 °C (300 °C for LPM), for 1 h. The LPM glass

was crushed into powder to be used as raw material for synthesizing **1** doped hybrid glass by spark plasma sintering (SPS).

Synthesis of inorganic glass and hybrid glass by SPS

Firstly, 0.5g LPM glass powder was weighed and load into the graphite die of 10 mm diameter using a sheet of Papyex® (flexible graphite sheet) to ensure the release of the solid as well as to protect the diffusion of the graphite component from the mold [16]. Some experiments which is detailed in supporting information Figure S1 lead to the conclusion that the optimal densification is obtained when sintering conditions are established at around 300 °C for 3 minutes under a pressure of 5 kN. Then, 1 mg of **1** were dissolved in around 5 ml acetone in a beaker, then 0.5 g LPM glass powder was added. After that, the beaker was disposed into an ultrasonic apparatus and processed for 20 minutes at 50 °C. Then, the beaker was put on a hot plate at around 50 °C to dry. After drying, the mixed powder was put in the agate mortar to grind. This is for getting a better homogeneity of the sample. Lastly, the powder was load into the graphite die, and the follow process is the same as described above.

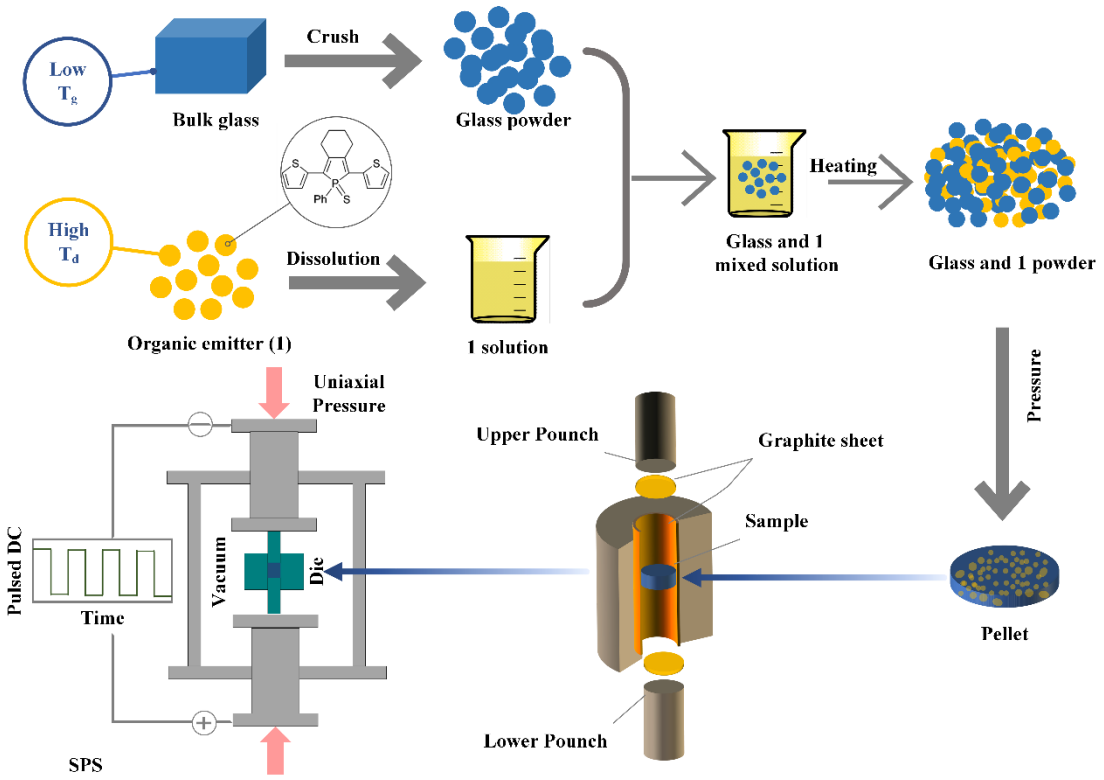

Figure 1. Schematic illustration for the synthesis of organic-inorganic hybrid glass

Characterizations

The DSC scans (TA Instruments SDT 2960) were carried out on samples of 10 mg in an Al pan. The overall accuracy of this measurement is expected to be within ±1 K. The T_g was determined at a heating rate of 10K/min. The amorphous nature of the prepared glasses were characterized by the X-ray diffraction measurements (XRD) (D/max 2550 VB/PC Rikagu, Japanese). All measurements were carried out at room temperature using Cu Kα radiation (λ=1.54056Å). A step size of 0.02°(2θ) was used with a scan speed of 2°/min. The electrochemical impedance spectroscopy (EIS) was characterized from the electrochemical station (Autolab PGSTAT302N). Before the measurement, two gold electrodes were deposited on both the surfaces of the glass sample (Leica EM ACE200) for 60 seconds. A stainless-steel plate covered by gold was attached

to both faces of the pellet as working and counter electrodes. The sample was put in a sealed cell connected to the electrochemical station and associated measuring devices. The transmittance spectrum of LPM was measured by UV-Vis spectrophotometer (JASCO V-570UV/VIS) ranging from 300 to 1000 nm. Microstructural analysis was performed by using transmission electron microscope (TEM, JEOL JEM 2100F). All-solid-state NMR experiments were performed using a Bruker 600 Avance III spectrometer (14T) using a Bruker triple-gramma 2.5 mm probe head operating at Larmor frequency of 242 MHz for ^{31}P. Magic Angle Spinning frequency was set to 20 kHz. ^{31}P NMR spectra were acquired using a single pulse sequence. The pulse length was set to 1.5 μs corresponding to a 90° flip angle with a repetition delay set to 30 s. The cyclic voltammetry was undertaken using a chemical station (Autolab PGSTAT302N) at a scanning rate of 0.2 mV/s between 2.1 and 2.3 V, and the other processes is similar to that of EIS measurement.

Results and Discussion

Inorganic glass electrolytes

As mentioned, the high resistance to thermal degradation is one of the main reasons for selecting the **1** in this work. Obviously, under the premise that the inorganic glass possesses an adequate ionic conductivity, the glass presenting low T_g is also essential for making hybrid glass. Binary lithium phosphate glasses are well known for being highly doped with Li^+ in order to increase their ionic conductivity [21]. However, the T_g of all the binary lithium phosphate glasses is higher than 300 °C, and the DSC results were shown in Figure S2. Fortunately, K. J. Rao has reported that the addition of sulphate ions into binary lithium phosphate glass can decrease the T_g and improve the ionic conductivity in the meantime [22]. Based on their study, the glass with composition of 25%Li_2SO_4-40%Li_2O-35%P_2O_5 (LPM) was selected as the glass host, and the chemical-physical

characteristics of the glass was investigated. Figure 2(a) shows that the T_g of the LPM is below 300 °C, which is indeed caused by the introduction of sulfur confirmed by the EDS analysis mapping as shown in Figure S3. This low T_g may allow for making hybrid materials combining phosphate glass and organic emitter by SPS densification below 300°C. The XRD pattern of the prepared phosphate glass indicates the glass is amorphous as shown in Figure 2(b). The peak at around 13° is contributed to the sample plate. Although some reports mention that the ionic conductivity of the glass would improve with the occurrence of crystal phase in the glass matrix, it is believed that the amorphous state host could promote the recombination of the hole and the electron within the electrolyte, which is beneficial to the electrochemical reaction of the LEC [3]. As shown in Figure 2(c), the optical window of the prepared glass starts at about 320 nm thus covering the full visible range, which indicates the corresponding bandgap is about 3.87 eV. The glass presents a high transmission of 85% without absorption bands in the working wavelength range. Moreover, the glass has high absorbance in UV range, which can prevent **1** from being damaged by the UV irradiation.

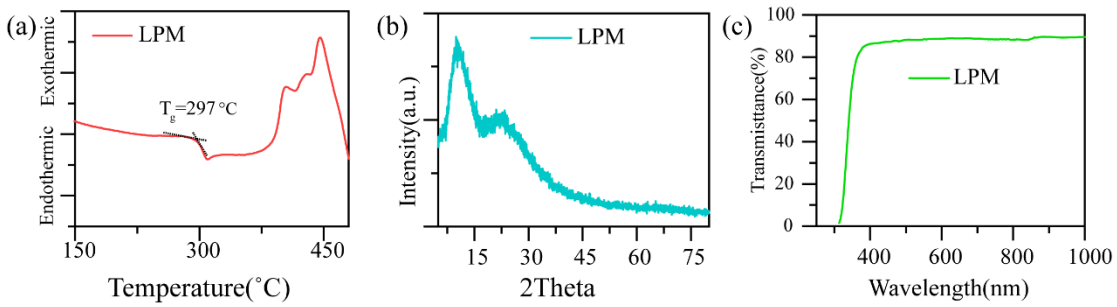

Figure 2. (a) DSC curve; (b) XRD pattern; (c) Transmittance spectrum; of the LPM glass

The temperature-dependent ionic conductivity of LPM is shown in Figure 3(a). A typical behaviour of ions transport glass solid electrolyte presenting a semicircle at high frequency and a spike at low-frequencies is observed. The semicircle is attributed to bulk conductivity, whereas the

spike is a product of space-charge polarization effects from the accumulation of ions at the electrodes[23]. The conductivity of the prepared Li phosphate glasses were also determined by the frequency dependent complex impedance, $\hat{z}(v)' = z'(v), +iz''(v)$. The real part of conductivity was calculated according to

$$\sigma'(v) = \frac{t}{A}\frac{Z'(v)}{[Z'(v)]^2 + [Z''(v)]^2} \quad (1)$$

where t is the thickness of the glass and A is the area of the electrode. Here, since just the DC conductivity was considered, the circuit resistance (R) equal to the real impedance $z'(v)$ when the imaginary impedance $z''(v)$ is at a local minimum at low frequencies(equal to about 0). Thus, the Eq(1) is approximately equal to

$$\sigma_{\mathrm{dc}} = \frac{\mathrm{t}}{RA} \quad (2)$$

where R is equal to $z'(v)$ and the fitting of ionic conductivity of the samples also obey well the Arrhenius law

$$\sigma_{\mathrm{dc}}T = A\exp\left(-\frac{E_{\mathrm{act}}}{\mathrm{k_B}T}\right) \quad (3)$$

Where A and E_{act} denote respectively the pre-exponential factor and the activation energy of the DC conductivity, while k_B is Boltzmann's constant. As shown in Figure 3(b), the ionic conductivity of the prepared glass can reach 10^{-7} S/cm at 297 K and 10^{-6} S/cm at 330 K, respectively, which is higher than that of binary lithium phosphate glasses as shown in Figure S4 and is comparable to that of the organic electrolyte used in LEC[24].

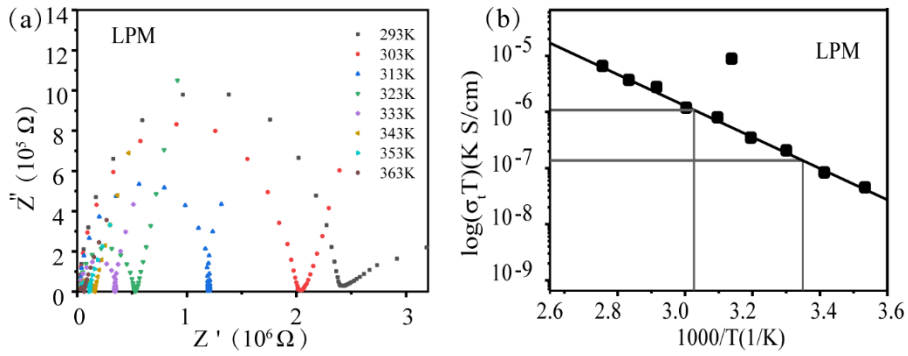

Figure 3. (a) Electrochemical impedance spectroscopy at different temperature and (b) ionic conductivity of the LPM glass

Inorganic glass and hybrid glass prepared by SPS

Firstly, the optimal sintering condition for LPM was investigated. The images of the glass samples with different sintering temperature and pressure are shown in Figure S2. It is found that the glass sample sintered at 298 °C for 3 minutes under the pressure of 5 kN, denoted as LPS, shows the best densification. Then, the **1** doped hybrid phosphate glass was also successfully obtained by SPS sintering at 298 °C with a pressure of 5 kN as shown in Figure 4(a). It can be seen that the hybrid glass is yellow and transparent, in agreement with the optical characteristic of the dopant. Figure 4(b) displays the strong photoluminescence of hybrid glass under 430 nm excitation. Although the T_g of LPM is still higher than the T_d of **1**, it is reasonable to point out that the **1** molecule fluorophore was not destroyed during the SPS sintering process, which suggests SPS technology can be an innovative route to synthesize organic-inorganic hybrid materials. The emission peak of the hybrid glass is at 600 nm, in the typical range of the emission of **1**, as shown in Figure 4(c).

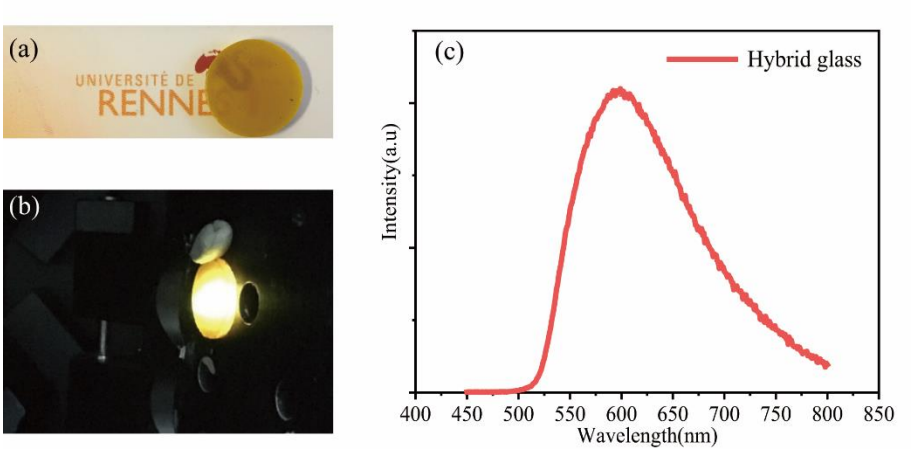

Figure 4. (a) Digital photo of the hybrid glass; (b) Digital photo of the hybrid glass under 430 nm excitation; (c) The photoluminescence spectrum of the hybrid glass under 430 nm excitation

TEM was performed to study the miscrostructure of the hybrid glass due to it is a feasible way to investigate the interface morphology of glass-ceramics. The TEM pictures of **1** doped hybrid glass are shown in Figure 5(a). Since the atomic mass of the **1** (mainly carbon) is much lower than the glass host (mainly P and O), the **1** is bright and the glass matrix is dark. It can be seen from Figure 5(a) that the aggregates of **1** are indeed homogeneously distributed in the glass matrix. As a contrast, the TEM images of the undoped LPS glass was also performed as shown in Figure 5(b), and no bright aggregates were observed in all the LPS glass sample pieces, which indicates that the bright aggregates are indeed **1**. Complementary TEM images are shown in Figure S5. The average size of the aggregates of **1** is of about 100 nm, which suggests the hybrid glass exhibits a minor phase separation on a sub-micron scale. This is probably because **1** have been aggregated when they separate out of the acetone during the heating process as shown in the Figure 1. Thus, a better mixing process of glass powder and **1** should be realized to obtain a better morphology of the hybrid glass, such as low-energy ball milling method.

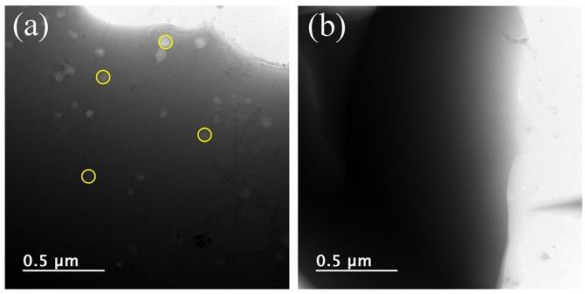

Figure 5. TEM images of the organic-inorganic hybrid glass(a) and inorganic glass matrix(b)

Moreover, the NMR study of the ^{31}P nucleus has been performed in the LPM, LPS and hybrid glass, the results are presented in Figure 6. The ^{31}P resonances and related parameters have been identified and all the chemical shifts are listed in Table 1.

Table 1 ^{31}P chemical shifts of LPM, LPS and the hybrid glass and the relative proportions of Q^1 and Q^2 species as determined by ^{31}P NMR

Sample		δ_{iso} (ppm)	FWHM (Hz)	δ_{CSA} (ppm)	δ_{CSA}	I(%)
LPM	Q^1	-3.4	2000	98	0.2	38
	Q^2	-21	3200	-125	0.6	62
LPS	Q^1	-3.2	2100	89	0.3	46
	Q^2	-20.2	3300	-117	0.9	54
Hybrid	Q^1	-3.3	2000	94	0.2	47
	Q^2	-20.2	3200	-124	0.5	53

Only two ^{31}P resonances are observed, and the chemical shift of -3 ppm and -20 ppm correspond to the contribution of Q^1 and Q^2 species, respectively [25-27]. As expected, no peaks of Q^3 species (chemical shift of -50 ppm) were observed. The ratio between Q^1 and Q^2 species is directly affected

by the synthesis process, passing from 38/62 for LPM to 46/54 for LPS and hybrid glass. This is probably because the glassy network is less polymerized for glasses prepared by SPS. Moreover, the linewidth is similar for the 3 samples (Q^1: about 2kHz and Q^2: about 3.2 kHz). That indicates that the local disorder is not impacted by the synthesis route or the presence of the molecule. The chemical shift tensor presents approximatively the same values for the 3 samples ((δ_{iso}, δ_{CSA} and η_{CSA} are quite similar for LPM, LPS and hybrid glass). So, the chemical environment is not affected by the synthesis process or by the presence of the **1**.

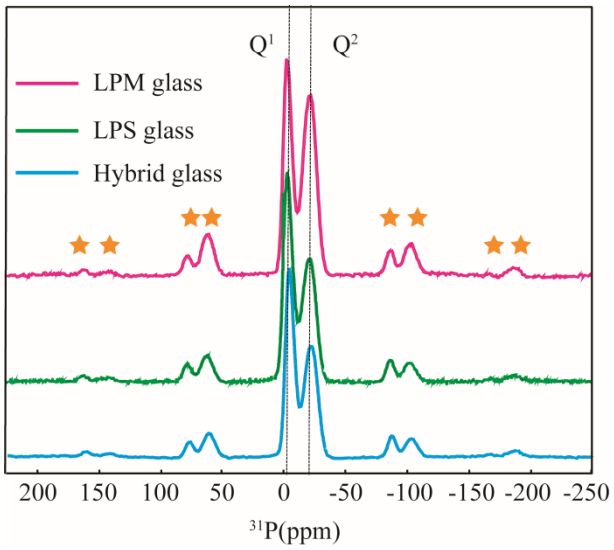

Figure 6. ^{31}P NMR of LPM, LPS and the hybrid glass. Spinning sidebands are indicated by stars

The ionic conductivity of the hybrid glass was determined by the complex impedance analysis and the corresponding Arrhenius plots were fitted as shown in Figure 7(a), LPS is shown as a reference. Unfortunately, both LPS (8.1×10^{-8} S/cm at RT) and hybrid glass (6.1×10^{-8} S/cm at RT) present a lower ionic conductivity than that of LPM (10^{-7} S/cm at RT), which may be caused by defects due to the sintering process such as impurities, residual pores and grain boundaries. Moreover, the ionic conductivity of the hybrid glass is slightly lower than that of LPS. Effectively, aggregates of **1** within the glass matrix can hinder the movement of lithium ions in the glass decreasing the ionic

conductivity. In fact, a single crystal or single amorphous phase material, without grain boundary, is the ideal medium for fast ionic conduction.[8] Therefore the phase separation between the glassy matrix and **1** in the hybrid glass is expected to be similar to the grain boundary behavior in the glass-ceramics[28].

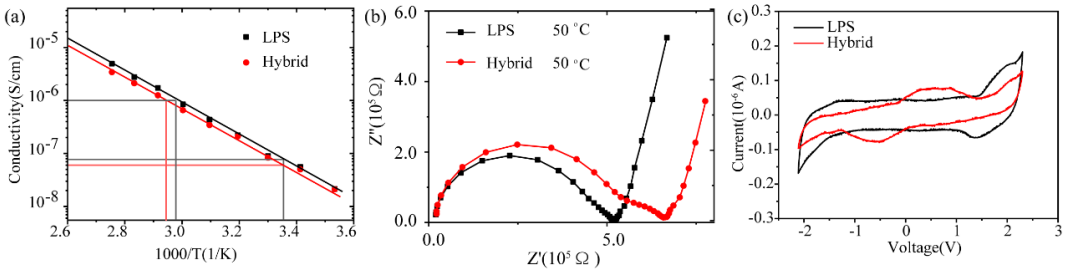

Figure 7. (a)Arrhenius plots of the dc conductivities of LPS and hybrid glass; (b) Nyquist plots of LPS and hybrid glass at 50 °C; (c) Cyclic voltammetry measurement of LPS and hybrid glass with a scanning rate of 0.2 mV/S at 50 °C

This explanation is supported by the complex impedance plots of the LPS glass and hybrid glasses. The complex impedance plots of LPS and hybrid glass at 50 °C (keep the ionic conductivity above 10^{-7} S/cm) are shown in Figure 7(b). Two semi-circles, can be distinguished at high frequency and a small one at low frequency, in the hybrid glass, which is not observed from other prepared glasses. According to other reports[28,29], this second semi-circle is a typical fingerprint of the grain boundary. Although there is no grain boundary in the glass matrix, the phase separation is probably causing a slight decrease in ionic conductivity.

Cyclic voltammetry (CV) measurement is used to determine the electrochemical stability window of the glass electrolyte as well as the electrochemical doping process of the **1**. As shown in Figure 7(c), visible anodic and cathodic currents respectively attributable to gold dissolution ($Au \rightarrow Au^{3+} + 3e^-$) and deposition ($Au^{3+} + 3e^- \rightarrow Au$) are observed in the potential range from 1.5 to 1.3 V,

which also shows good reversibility. In addition, the current due to electrolyte decomposition is detected in the range -2V/2 V. In the hybrid glass, besides the observed peaks, a redox couple was observed. Although the oxidation peak (E_{pa}) and reduction peak (E_{pc}) of **1** have been measured in CH_2Cl_2, referenced to Fc/Fc^+ half cell [30], the simple contrasting method does not work since the measurement condition is different. Compared to the result of LPS, this redox couple is mainly due to the contribution of **1**. This suggests that **1** can complete the exchange of electric charges [3], which is a fingerprint of the transient phenomena of a LEC. However, because of the complex dynamic reaction process of LEC, the present results are not able to complete support that the inorganic glass electrolytes can be utilized in a LEC. Obviously, further works need to be done to unravel this question such as 1) to fabricate a thin hybrid glass (thickness < 50μm); 2) to improve the doping homogeneity; 3) to find glass electrolyte with higher ionic conductivity; 4) to find a more proper method for the synthesis of hybrid glass, for example, using a Sol-gel process.

Conclusion

To conclude, we have successfully synthesized **1** doped hybrid glass which appears to be a promising active material for LEC through SPS method. Strong photoluminescence characteristic of the organic emitter (π-extended phosphole sulfide **1**) was observed in the hybrid glass. The organic emitter is not destroyed during the sintering process, which is further confirmed by the TEM picture of the hybrid glass. Aggregates of **1** were directly observed in the hybrid glass through TEM images, and the average size of the aggregates is of about 100 nm. Moreover, the ionic conductivity of the hybrid glass is lower than that of LPS glass, and a “grain boundary” between the glass matrix and **1** was observed. The redox couple contributed to **1** was determined by the CV of the hybrid glass, suggesting that **1** can complete the chemical doping process. This

doping process is a fingerprint of the transient phenomena of a LEC. However, further works need to be done to confirm that hybrid glass electrolytes can be used to prepare efficient LEC.

Funding

Natural Science Foundation of Zhejiang Province(Q21F050026); European Regional Development Fund (ERDF); Ministry of Higher Education and Research, the French region of Brittany and Rennes Métropole.

Acknowledgement

Authors also would like to acknowledge the IUF (Institut Universitaire de France) and China Scholarship Council (CSC).

Notes

The authors declare no competing financial interest.

Author contribution statement：

Muzhi CAI: Investigation, Writing - original draft, Writing - review & editing.

Laurent Calvez: Conceptualization，Methodology, Formal analysis, Validation.

Jean Rocherulle: Conceptualization, Formal analysis, Validation.

Pierre-Antoine Bouit: Synthesis of organic molecule, Formal analysis, Validation.

Muriel Hissler: Synthesis of organic molecule, Formal analysis.

Hongli Ma: Formal analysis, Validation.

Claire Roiland: NMR analysis.

Vincent Dorcet: TEM analysis.

Junjie Zhang: Formal analysis, Validation.

Shiqing Xu: Formal analysis, Validation, Project administration.

Xianghua Zhang: Project administration.

Reference

[1] Q. Pei, G. Yu, C. Zhang, Y. Yang, A.J. Heeger, Polymer light-emitting electrochemical cells, Science 269(5227) (1995) 1086-1088. https: //doi.org/ 10.1126/science.269.5227.1086

[2] S.B. Meier, D. Tordera, A. Pertegás, C. Roldán-Carmona, E. Ortí, H.J. Bolink, Light-emitting electrochemical cells: recent progress and future prospects, Mater. Today 17(5) (2014) 217-223. https://doi.org/10.1016/j.mattod.2014.04.029

[3] S. van Reenen, M. Kemerink, Light-Emitting Electrochemical Cells: Mechanisms and Formal Description, Light-Emitting Electrochemical Cells 2017, pp. 3-45.

[4] S. Tang, A. Sandstrom, P. Lundberg, T. Lanz, C. Larsen, S. van Reenen, M. Kemerink, L. Edman, Design rules for light-emitting electrochemical cells delivering bright luminance at 27.5 percent external quantum efficiency, Nat. Commun. 8(1) (2017) 1190. https://doi.org/10.1038/s 41467-017-01339-0

[5] J.D. Slinker, J.A. DeFranco, M.J. Jaquith, W.R. Silveira, Y.W. Zhong, J.M. Moran-Mirabal, H.G. Craighead, H.D. Abruna, J.A. Marohn, G.G. Malliaras, Direct measurement of the electric-field distribution in a light-emitting electrochemical cell, Nat. Mater. 6(11) (2007) 894-9. https://

doi.org/10.1038/nmat2021

[6] L.S. Pingree, D.B. Rodovsky, D.C. Coffey, G.P. Bartholomew, D.S. Ginger, Scanning kelvin probe imaging of the potential profiles in fixed and dynamic planar LECs, J. Am. Chem. Soc. 129(51) (2007) 15903-15910. https://doi.org/10.1021/ja074760m

[7] D.B. Rodovsky, O.G. Reid, L.S. Pingree, D.S. Ginger, Concerted emission and local potentiometry of light-emitting electrochemical cells, Acs Nano 4(5) (2010) 2673-2680. https://doi.org/10.1021/nn1003315

[8] S. van Reenen, P. Matyba, A. Dzwilewski, R.A. Janssen, L. Edman, M. Kemerink, A unifying model for the operation of light-emitting electrochemical cells, J. Am. Chem. Soc. 132(39) (2010) 13776-13781. https://doi.org/10.1021/ja1045555

[9] S. Tang, L. Edman, Light-Emitting Electrochemical Cells: A Review on Recent Progress, Top. Curr. Chem 374(4) (2016) 40. https://doi.org/10.1007/978-3-319-59304-3_12

[10] F. AlTal, J. Gao, Long-term testing of polymer light-emitting electrochemical cells: Reversible doping and black spots, Org. Electron. 18 (2015) 1-7. https://doi.org/10.1016/j.orgel.2014.12.028

[11] A. Asadpoordarvish, A. Sandström, S. Tang, J. Granström, L. Edman, Encapsulating light-emitting electrochemical cells for improved performance, Appl. Phys. Lett. 100(19) (2012) 193508. https://doi.org/10.1063/1.4714696

[12] S. Tang, L. Edman, Quest for an Appropriate Electrolyte for High-Performance Light-Emitting Electrochemical Cells, J. Phys. Chem. Lett. 1(18) (2010) 2727-2732. https://doi.org /10.1021/jz1010797

[13] J. Mindemark, S. Tang, H. Li, L. Edman, Ion Transport beyond the Polyether Paradigm:

Introducing Oligocarbonate Ion Transporters for Efficient Light-Emitting Electrochemical Cells, Adv. Funct. Mater. 28(32) (2018) 1801295. https://doi.org /10.1002/adfm.201801295

[14] J. Ràfols-Ribé, N.D. Robinson, C. Larsen, S. Tang, M. Top, A. Sandström, L. Edman, Self-Heating in Light-Emitting Electrochemical Cells, Adv. Funct. Mater. 30(33) (2020) 1908649. https://doi.org/10.1002/adfm.201908649

[15] E. Fresta, M.A. Monclús, M. Bertz, C. Ezquerro, J.M. Molina-Aldareguia, J.R. Berenguer, M. Kunimoto, T. Homma, R.D. Costa, Key Ionic Electrolytes for Highly Self-Stable Light-Emitting Electrochemical Cells Based on Ir(III) Complexes, Adv. Opt. Mater. 8(12) (2020) 2000295. https://doi.org/10.1002/adom.202000295

[16] M. Hubert, E. Petracovschi, X.H. Zhang, L. Calvez, Synthesis of Germanium–Gallium–Tellurium (Ge–Ga–Te) Ceramics by Ball-Milling and Sintering, J. Am. Ceram. Soc. 96(5) (2013) 1444-1449. https://doi.org/10.1111/jace.12299

[17] Fave C, Hissler M, Sénéchal K, et al. Ligand trans-effect: using an old concept as a novel approach to bis (dipolar) NLO-phores, Chem. Commun. 2002 (16): 1674-1675. https://doi.org/10.1039/b203149c

[18]Hong Y, Lam J W Y, Tang B Z. Aggregation-induced emission, Chem. Soc. Rev. 2011 40(11): 5361-5388. https://doi.org/10.1039/C1CS15113D

[19] Richard K B. Review: the structure of simple phosphate glasses, J. Non-Cryst. Solids 2000 263: 1-28. http://dx.doi.org/10.1016/S0022-3093(99)00620-1

[20] Su H C, Fadhel O, Yang C J, et al. Toward functional π-conjugated organophosphorus materials: design of phosphole-based oligomers for electroluminescent devices, J. Am. Chem. Soc.

2006, 128(3): 983-995. https://doi.org/10.1021/ja0567182

[21] Martin S W. Ionic conduction in phosphate glasses, J. Am. Chem. Soc. 1991, 74(8): 1767-1784. https://doi.org/10.1111/j.1151-2916.1991.tb07788.x

[22] Ganguli M, Rao K J. Studies of ternary Li_2SO_4–Li_2O–P_2O_5 glasses, J. Non-Cryst. Solids 1999, 243(2-3): 251-267. https://doi.org/10.1016/S0022-3093(98)00832-1

[23] R. Christensen, G. Olson, S.W. Martin, Ionic Conductivity of Mixed Glass Former 0.35 Na_2O + 0.65 [x B_2O_3+(1–x) P_2O_5] Glasses, J. Phys. Chem. B 117(51) (2013) 16577-16586. https://doi.org/10.1021/jp409497z

[24] S. van Reenen, T. Akatsuka, D. Tordera, M. Kemerink, H.J. Bolink, Universal transients in polymer and ionic transition metal complex light-emitting electrochemical cells, J. Am. Chem. Soc 135(2) (2013) 886-91. https://doi.org/10.1021/ja3107803

[25] R. Morena, Phosphate glasses as alternatives to Pb-based sealing frits, J. Non-Cryst. Solids 263 (2000) 382-387. https://doi.org/10.1016/S0022-3093(99)00678-X

[26] R.K. Brow, C.C. Phifer, G.L. Turner, R.J. Kirkpatrick, Cation effects on ^{31}P MAS NMR chemical shifts of metaphosphate glasses, J. Am. Ceram. Soc. 74(6) (1991) 1287-1290. https://doi.org/10.1111/j.1151-2916.1991.tb04099.x

[27] P. Losso, B. Schnabel, C. Jäger, U. Sternberg, D. Stachel, D. Smith, ^{31}P NMR investigations of binary alkaline earth phosphate glasses of ultra phosphate composition, J. Non-Cryst. Solids 143 (1992) 265-273. https://doi.org/10.1016/S0022-3093(05)80576-9

[28] T. Van Dijk, A. Burggraaf, Grain boundary effects on ionic conductivity in ceramic $Gd_xZr_{1-x}O_{2-(x/2)}$ solid solutions, Phys. Status Solidi A 63(1) (1981) 229-240. https://doi.org/10.1002

/pssa.2210630131

[29] J. Fu, Superionic conductivity of glass-ceramics in the system Li_2O-Al_2O_3-TiO_2-P_2O_5, Solid State Ionics 96(3-4) (1997) 195-200. https://doi.org/10.1016/S0167-2738(97)00018-0

[30] C. Fave, T.-Y. Cho, M. Hissler, C.-W. Chen, T.-Y. Luh, C.-C. Wu, R. Réau, First examples of organophosphorus-containing materials for light-emitting diodes, J. Am. Chem. Soc. 125(31) (2003) 9254-9255. https://doi.org/10.1021/ja035155w